NUMERICAL SOLUTION FOR WOOD DRYING ON ONE-DIMENSIONAL GRID

YONG HUN LEE, WOOK KANG, AND WOO YANG CHUNG

ABSTRACT. A mathematical modeling for the drying process of hygroscopic porous media, such as wood, has been developed in the past decades. The governing equations for wood drying consist of three conservation equations with respect to the three state variables, moisture content, temperature and air density. They are involving simultaneous, highly coupled heat and mass transfer phenomena. In recent, the equations were extended to account for material heterogeneity through the density of the wood and via the density variation of the material process, capillary pressure, absolute permeability, bound water diffusivity and effective thermal conductivity. In this paper, we investigate the drying behavior for the three primary variables of the drying process in terms of control volume finite element method to the heterogeneous transport model on one-dimensional grid.

1. INTRODUCTION

Drying is one of the most complex phenomena happened in engineering because of the simultaneous heat and mass transfer taking place in the course of the process. In the past decades, many researchers developed drying models of porous media, in particular, wood. Wood drying is more difficult than other porous media such as concrete and brick, because it has the anisotropic and heterogeneous characteristic. Although the investigation of the drying processes has been realized both experimentally and theoretically for centuries, the coupling of heat and mass transfer and other phenomena in drying is still a challenging problem.

In developing a drying model based on the continuous approach, Whitaker[12, 13] used the volume averaging technique to derive a system of macroscopic transport equations from a set of basic transport laws at microscopic level(pore scale) for the three phases(gas, liquid and solid). He assumed that a porous medium was to be equivalent

to a continuum. A system of conservation equations for mass, energy and momentum was introduced using average state variables. His continuous model is considered as rigorous and the most advanced continuous model today.

Based on the Whitaker's theory, a mathematical modelling of the wood drying is developed by many authors, for example, Perré and Turner [4, 5, 7]. Also the numerical simulation for the drying process was developed using derived average conservation equations [1, 2, 3, 8, 11]. Among others, Perré and Turner employed the control volume finite element method(CVFEM) to solve the system of transport equations. The main advantage of CVFEM is that it ensures the conservation of mass and enthalpy through the boundary of each control volume as well as whole domain. However it has some difficulties due to mathematical complexity of the governing equations.

In this paper, we implement the heterogeneous and highly coupled heat and mass transfer modelled by Perré and Turner in the literature of CVFEM. In this model, the capillary pressure, the liquid and gas permeability, the effective diffusivity and effective thermal conductivity are very important coefficients. These parameters are normally functions of one or all state variables and depend on material characteristics. We compute this parameters by using the published values of corresponding primary state variables.

2. Mathematical Modelling

In this section, we introduce the mathematical formulation which represents the process of the wood drying, based on the model developed by Whitaker [12] and later by Perré and Turner [5]. The volume averaging method is applied to derive a continuous drying model for wood at macroscopic level. The wood consists of three phases, free water, gas(air and water vapor) and solid. Solid includes the bound water.

The conservation equation is typically represented by the following:

$$\frac{\partial \varphi}{\partial t} + \nabla \cdot (\varphi \bar{\mathbf{v}} - \bar{\bar{\mathrm{D}}} \nabla \varphi) = 0,$$

where φ is the state variables, and $\bar{\mathbf{v}}$ is velocity vector and $\bar{\bar{\mathrm{D}}}$ effective diffusivity tensor.

The process of the wood drying is governed by three macroscopic conservation equations [6, 10]. The equations were extended to account for material heterogeneity through the density of the wood and via density variation of the material properties, capillary pressure, absolute permeability, bound liquid diffusivity and effective thermal conductivity. The system of the three governing equations is summarized as follows:

Liquid Mass Conservation:

$$\frac{\partial}{\partial t}(\rho_0 X + \varepsilon_{\mathrm{g}} \rho_{\mathrm{v}}) + \nabla \cdot (\rho_{\mathrm{w}} \bar{\mathbf{v}}_{\mathrm{w}} + \rho_{\mathrm{v}} \bar{\mathbf{v}}_{\mathrm{g}} - \rho_0 \bar{\bar{\mathrm{D}}}_{\mathrm{b}} \nabla X_{\mathrm{b}}) = \nabla \cdot (\rho_{\mathrm{g}} \bar{\bar{\mathrm{D}}}_{\mathrm{v}} \nabla w_{\mathrm{v}}),$$

Energy Conservation:

$$\frac{\partial}{\partial t}\Big(\rho_0(Xh_{\mathrm{w}} + h_{\mathrm{s}}) + \varepsilon_{\mathrm{g}}(\rho_{\mathrm{v}}h_{\mathrm{v}} + \rho_{\mathrm{a}}h_{\mathrm{a}}) - \int_0^{\rho_0 X_{\mathrm{b}}} \Delta h_{\mathrm{w}} d\rho - \varepsilon_{\mathrm{g}}P_{\mathrm{g}}\Big)$$

$$+\nabla \cdot (\rho_{\mathrm{w}}h_{\mathrm{w}}\bar{\mathbf{v}}_{\mathrm{w}} + (\rho_{\mathrm{v}}h_{\mathrm{v}} + \rho_{\mathrm{a}}h_{\mathrm{a}})\bar{\mathbf{v}}_{\mathrm{g}} - h_{\mathrm{b}}\rho_0\bar{\bar{\mathrm{D}}}_{\mathrm{b}}\nabla X_{\mathrm{b}})$$

$$= \nabla \cdot (\rho_{\mathrm{g}}\bar{\bar{\mathrm{D}}}_{\mathrm{v}}(h_{\mathrm{v}}\nabla w_{\mathrm{v}} + h_{\mathrm{a}}\nabla w_{\mathrm{a}}) + \bar{\bar{\mathrm{K}}}_{\mathrm{eff}}\nabla T),$$

Air Conservation:

$$\frac{\partial}{\partial t}(\varepsilon_{\mathrm{g}}\rho_{\mathrm{a}}) + \nabla \cdot (\rho_{\mathrm{a}}\bar{\mathbf{v}}_{\mathrm{g}}) = \nabla \cdot (\rho_{\mathrm{g}}\bar{\bar{\mathrm{D}}}_{\mathrm{v}}\nabla w_{\mathrm{a}}).$$

The primary variables in system are the moisture content X, the temperature T and the intrinsic phase air density $\bar{\rho}_{\mathrm{a}}$, where:

$$\bar{\rho}_{\mathrm{a}} = \varepsilon_{\mathrm{g}}\rho_{\mathrm{a}}.$$

Here the moisture content X contains the bound water X_{b}, i.e.,

$$X = X_{\mathrm{w}} + X_{\mathrm{b}}, \quad X_{\mathrm{w}} = \frac{\varepsilon_{\mathrm{w}}\rho_{\mathrm{w}}}{\rho_0}, \quad X_{\mathrm{b}} = \min(X, X_{\mathrm{fsp}}),$$

where X_{w} is free water.

The remaining symbols are secondary variables and parameters, where ρ represents density, ε the volume fraction, $\bar{\mathbf{v}}$ the phase velocity, ω the mass fraction, h the enthalpy and P the pressure. The subscript $\mathrm{a,b,g,s,v,w}$ represent the air, bound water, gas, solid(cell wall), vapor and water(or liquid) phases, respectively. The density of the wood is represented by ρ_0 and the effective vapor diffusivity, bound water diffusivity and effective thermal conductivity are represented by $\bar{\bar{\mathrm{D}}}_{\mathrm{v}}$, $\bar{\bar{\mathrm{D}}}_{\mathrm{b}}$ and $\bar{\bar{\mathrm{K}}}_{\mathrm{eff}}$, respectively and $\bar{\mathbf{v}}_{\mathrm{w}}$ and $\bar{\mathbf{v}}_{\mathrm{g}}$ are the liquid and gaseous phase velocities, respectively, given by the generalized Darcy's law:

$$\bar{\mathbf{v}}_{\ell} = -\bar{\bar{\mathrm{K}}}_{\ell}\frac{\bar{\bar{\mathrm{k}}}_{\ell}}{\mu_{\ell}}\nabla\varphi_{\ell}, \qquad \nabla\varphi_{\ell} = \nabla P_{\ell} - \rho_{\ell}\mathrm{g}\chi,$$

where $\ell = \mathrm{w,g}$ and χ is the depth scalar.

For the sake of computation, we consider the one-dimensional virtual board sample which is flat sawn board cut from a soft wood species, as depicted by Figure 1. Also the computational meshes are generated by dividing evenly spaced within the board. The board size is 0.04m and as a result of the symmetry, the computational domain is 0.02m. The density for each node ranges from 252Kg/m^3 in the earlywood to 1016Kg/m^3 in the latewood, where the average density is 529.64Kg/m^3. The distribution of the density is shown in Figure 1.

Two end boundaries of the virtual board sample has the different type. The right end is external boundary and the left end is symmetric boundary. The boundary conditions
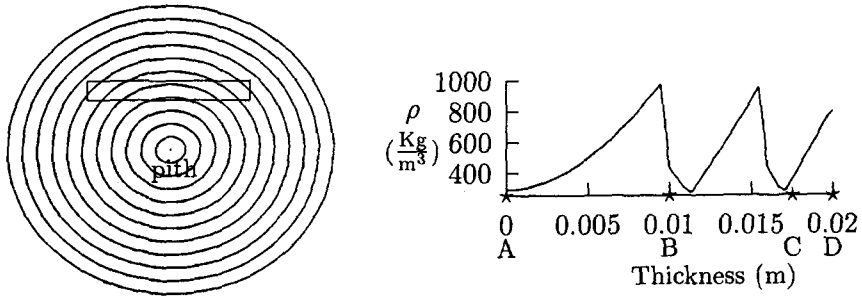
FIGURE 1. The virtual board description and the distribution of the density

proposed for the external drying surfaces are given as

$$\mathbf{J}_{\mathrm{w}} \cdot \hat{\mathbf{n}} = k_{\mathrm{m}} c M_{\mathrm{v}} \ln \left(\frac{1 - x_{\mathrm{v}\infty}}{1 - x_{\mathrm{v}}} \right),$$

$$\mathbf{J}_{\mathrm{e}} \cdot \hat{\mathbf{n}} = q(T - T_{\infty}) + h_{\mathrm{v}} k_{\mathrm{m}} c M_{\mathrm{v}} \ln \left(\frac{1 - x_{\mathrm{v}\infty}}{1 - x_{\mathrm{v}}} \right),$$

$$P_{\mathrm{g}} = P_{\infty},$$

where $\mathbf{J}_{\mathrm{w}}$ and $\mathbf{J}_{\mathrm{e}}$ represent the fluxes of liquid and energy at the boundary, respectively, $\hat{\mathbf{n}}$ is the outward unit normal vector, h_{v} and k_{m} the heat and mass transfer coefficients, respectively, x_{v} and $x_{\mathrm{v}\infty}$ the molar fractions of vapor at the exchange surface and in the air, respectively, and c the molar concentration. The pressure at the external drying surface is given at the atmospheric pressure. At symmetric boundary, all fluxes of liquid, heat, vapor and air are set to zero.

Also, we need some of initial conditions. The initial average moisture content $\bar{X}$ and temperature T are given by 120% and 25°C, respectively. Then initial moisture content distribution has to be determined prior to the commencement of the drying process. The liquid saturation $S_{\mathrm{w}i}(, i = 1, \ldots, N)$ at each node and the equilibrium capillary pressure P_{ceqm} are calculated from the nonlinear system of $(N + 1)$ equations as follows:

$$P_c(S_{\mathrm{w}i}, \rho_{oi}, T) = P_{\mathrm{ceqm}}, \quad i = 1, \ldots, N$$

$$\rho_{\mathrm{w}} \frac{\sum_i \phi_i S_{\mathrm{w}i} A_i}{\sum_i \rho_{oi} A_i} + X_{\mathrm{fsp}} = \bar{X},$$

where A_i is the area corresponding to the node i. Once the values of $S_{\mathrm{w}i}$ have been determined using Newton iteration, the initial moisture content can be calculated using:

$$X_i = \frac{\rho_{\mathrm{w}} \phi_i S_{\mathrm{w}i}}{\rho_{oi}} + X_{\mathrm{fsp}}, \quad i = 1, \ldots, N$$
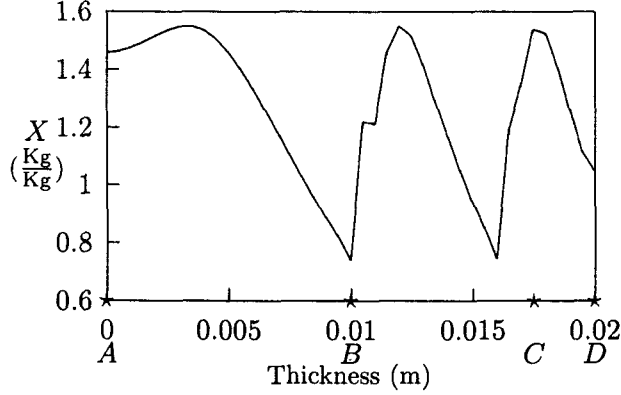
FIGURE 2. Initial distribution of moisture content

The computed moisture content ranged from 66% to 155%. In earlywood regions with lower density higher moisture contents occurs and in latewood regions with higher density moisture content is lower as depicted in Figure 2.

For the computation of drying process, we also need a suitable drying schedule. The dry and wet bulb temperatures were ramped up to their kiln operating values of 60°C and 40°C, respectively, over a period of 10 minutes.

3. CONTROL VOLUME FINITE ELEMENT METHODS

In this section we introduce CVFEM which is used to discretize the transport model. First, we recast three conservation equations to typical formulation as following:

$$(3.1) \qquad \frac{\partial}{\partial t}\Psi + \nabla \cdot \mathbf{J} = 0,$$

where Ψ represents conserved quantities $\rho_0 X + \varepsilon_g \rho_v$, $\rho_0(X h_w + h_s) + \varepsilon_g(\rho_v h_v + \rho_a h_a) - \int_0^{\rho_0 X_b} \Delta h_w d\rho - \varepsilon_g P_g$ or $\varepsilon_g \rho_a$ and $\mathbf{J}$ represents fluxes

$$\mathbf{J_w} = \rho_w \bar{\mathbf{v}}_w + \rho_v \bar{\mathbf{v}}_g - \rho_0 \bar{\bar{\mathbf{D}}}_b \nabla X_b - \rho_g \bar{\bar{\mathbf{D}}}_v \nabla w_v,$$

$$\mathbf{J_e} = \rho_w h_w \bar{\mathbf{v}}_w + (\rho_v h_v + \rho_a h_a)\bar{\mathbf{v}}_g - h_b \rho_0 \bar{\bar{\mathbf{D}}}_b \nabla X_b$$
$$\qquad - \rho_g \bar{\bar{\mathbf{D}}}_v(h_v \nabla w_v + h_a \nabla w_a) - \bar{\bar{\mathbf{K}}}_{\text{eff}} \nabla T,$$

$$\mathbf{J_a} = \rho_a \bar{\mathbf{v}}_g - \rho_g \bar{\bar{\mathbf{D}}}_v \nabla w_a.$$

Applying time discretization technique such as the backward Euler or the Crank-Nicolson schemes to (3.1), we have the following stationary equation at each time step

$$(3.2) \qquad (\Psi - \Psi^{(\text{prev})})/\delta t + \nabla \cdot \mathbf{J} = 0,$$

where $\Psi^{(\text{prev})}$ means the value of the conserved quantity at the previous time step. δt means the time step size.
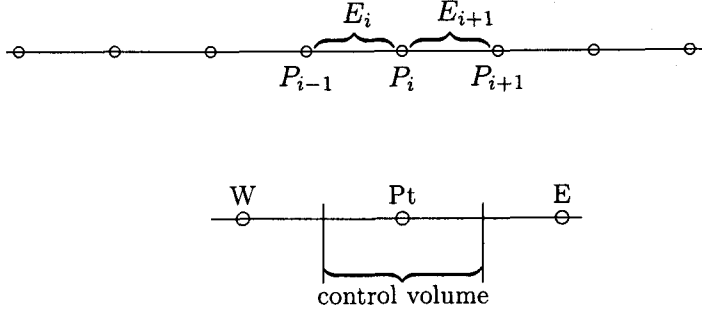
FIGURE 3. Construction of a one-dimensional finite elements and nodes(top) and control volumes(bottom).

As shown in Figure 3, the computational domain is meshed with subinterval elements, and at each node the control volumes(CVs) are constructed. To obtain the discretized formulation of the stationary equation (3.2), we have integrating over the each CV

$$\frac{\text{Area(CV)}}{\delta t}(\Psi_{\text{pt}} - \Psi_{\text{pt}}^{(\text{prev})}) + \int_{\text{CV}} \nabla \cdot \mathbf{J} \, dS = 0,$$

where Ψ_{pt}, the value of Ψ at the node point pt, is representative value of Ψ in the CV, i.e.,

$$\Psi_{\text{pt}} = \frac{1}{\text{Area(CV)}} \int_{\text{CV}} \Psi \, dS,$$

and applying the Gauss divergence theorem:

$$\alpha \Psi_{\text{pt}} + \sum_{f \in \mathfrak{F}_{\text{CV}}} (\mathbf{J} \cdot \mathbf{n})_f = \alpha \Psi_{\text{pt}}^{(\text{prev})},$$

where $\alpha = \frac{\text{Area(CV)}}{\delta t}$, $\mathfrak{F}_{\text{CV}}$ is the set of two end-points of the CV and $\mathbf{n}_f$ is outward unit normal vector. Also the term $(\mathbf{J} \cdot \mathbf{n})_f$ is evaluated accurately at the end-point of the CV. In order to evaluate the approximated value of the flux, we use different method for the advection and the diffusion terms. The finite element shape functions are used for the evaluation of the diffusion terms. For examples, the bound liquid diffusivity and the gradient of the bound water gives:

$$\bar{\bar{\mathbf{D}}}_{\text{b}} = \sum_{i=1}^{2} N_l \bar{\bar{\mathbf{D}}}_{\text{b}l}, \qquad \nabla X_{\text{b}} = \sum_{l=1}^{2} \nabla N_l X_{\text{b}l},$$

where the N_l are the shape function for a subinterval element containing the end-point of the CV and l denotes the nodes of this element. Also, for the advection terms, only

$\bar{\mathbf{v}}_w$ and $\bar{\mathbf{v}}_g$, the flux limiting method is used generally [9]. Then we have the $3N$ discrete analogue of the equations(3.2) as following:

$$F_{\text{pt}}(x) :=$$

(3.3) $$\alpha(\Psi_{\text{pt}}^{(n+1)} - \Psi_{\text{pt}}^{(n)}) + \alpha_{Pt}\mathbf{J}_{\text{pt}}^{(n+1)} + \alpha_W\mathbf{J}_W^{(n+1)} + \alpha_E\mathbf{J}_E^{(n+1)} = 0,$$

where the superscript $(n+1)$ means the current time level $t^{(n+1)}$, (n) the previous time level $t^{(n)}$, and time step size is $\delta t = t^{(n+1)} - t^{(n)}$.

4. Numerical Results

As explained above, we find the numerical solution by solving the transport equations in terms of control volume finite element methods. The transport coefficients that are necessary for numerical computation were referred to Truscott and Turner [11].

The discretized formulation (3.3) with boundary conditions is highly coupled system of nonlinear equations. Then we use the inexact Newton iterative method to solve this system.

$$\mathbf{x}^{(0)} : \text{ Initial iterate}$$
$$\text{For } n = 0, 1, \ldots, \text{ until } \|\mathbf{F}(\mathbf{x}^{(n)})\| < \text{ tolerance}$$
$$\text{Solve } \nabla_h\mathbf{F}(\mathbf{x}^{(n)})\delta\mathbf{x}^{(n)} = \mathbf{F}(\mathbf{x}^{(n)})$$
$$\mathbf{x}^{(n+1)} = \mathbf{x}^{(n)} - \delta\mathbf{x}^{(n)},$$

where the matrix $\nabla_h\mathbf{F}(\mathbf{x})$ is the difference approximation to the Jacobean matrix $\mathbf{F}'(\mathbf{x}) = (\frac{\partial F_j}{\partial x_i})$, and we can use the Bi-CGSTAB method to solve linear system. We can also use the Block TDMA solver because the Jacobean matrix is block tridiagonal matrix.

Figure 4 shows the drying kinetics during 20 hours. The left figures plot the behaviors of the average values and the right figures plot the behaviors at the four positions. The position A is the symmetric boundary, and the position D is the external drying boundary and the position B(0.01) is located in the latewood which has higher density, and the position C(0.0175) is located in the earlywood which has lower density.

The free water begins to move the evaporative free surface at the beginning of drying and remains the constant rate of drying until the free water movement stops, which is called to the constant drying rate period or funicular state. After the funicular state, a drying front recedes toward the interior of wood and the drying rate begin to decrease, which is called to the falling rate drying period or pendular state.

Figure 5 shows the spatial evolution of moisture content, gas pressure, and temperature distribution during drying. The effect of growth rings on moisture distribution is evident during drying as expected. The moisture content of earlywood locations decreases steadily from the beginning of drying but one of latewood locations remains constant up to 48 hour. The surface moisture content comes to the equilibrium state after drying time 4 hour but the surface temperature does not come to the equilibrium
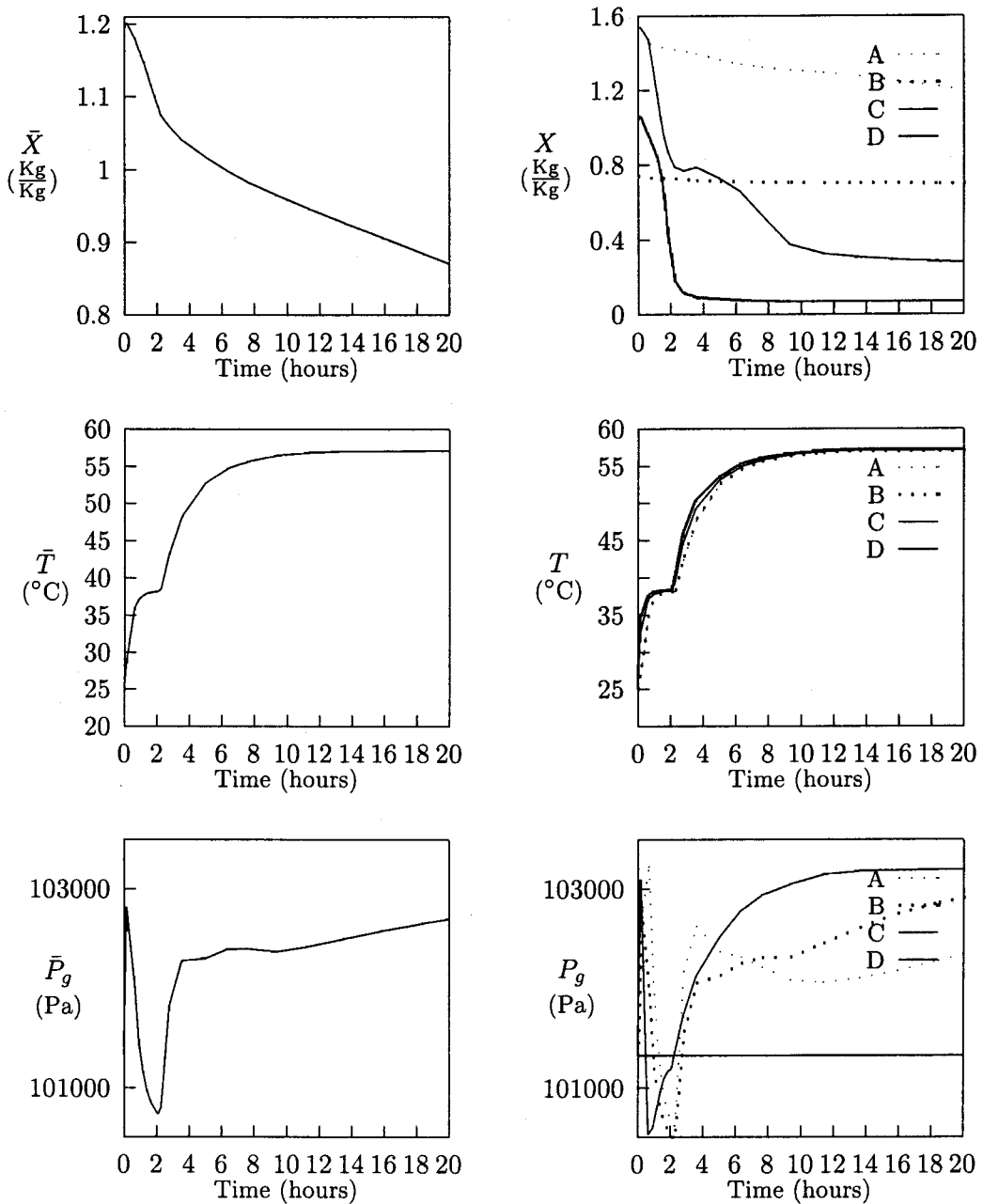
FIGURE 4. Average values(Left) and location values(Right) of Moisture contents, Temperature and Gas Pressure during 20 hours.
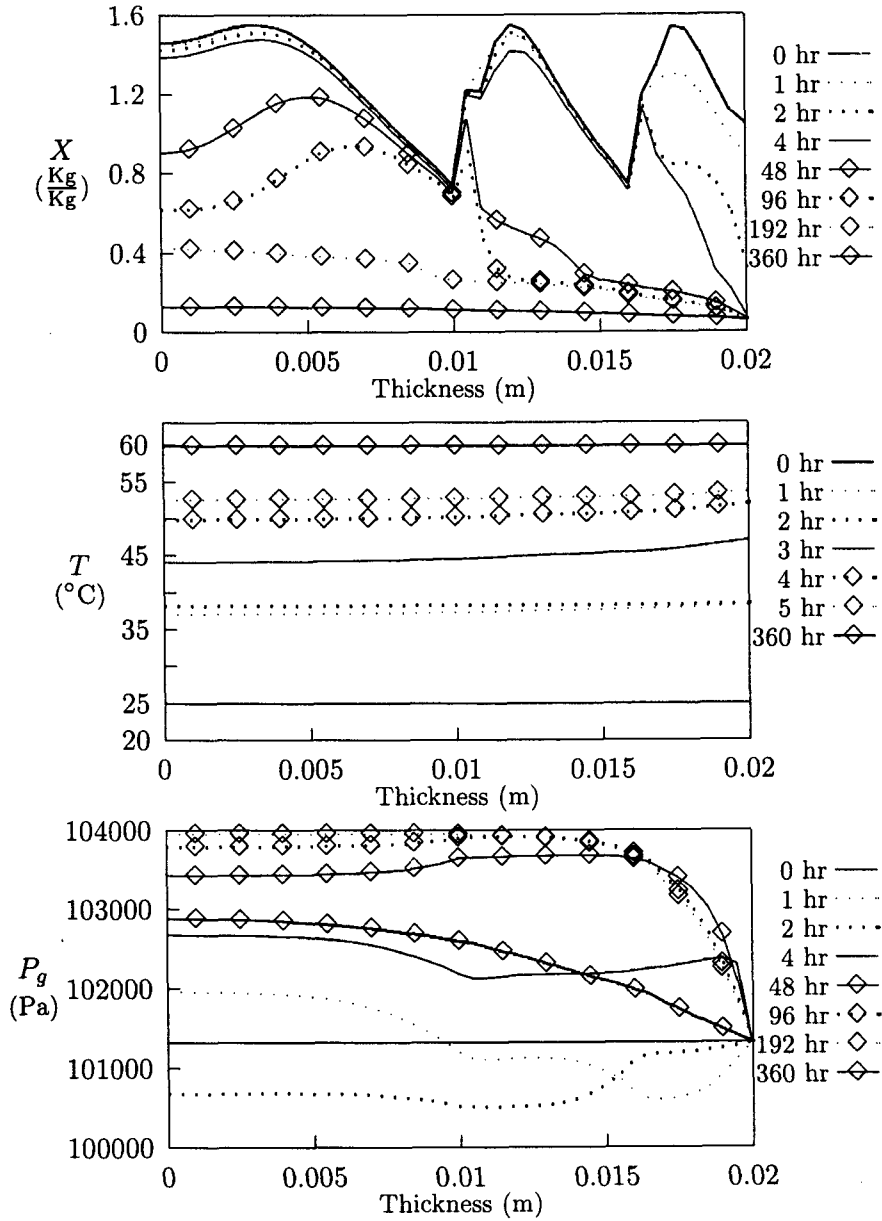
FIGURE 5. Spatial evolution of moisture content, temperature and gas pressure distribution during drying

state and approaches steadily to the dry bulb temperature due to the effect of the latent heat of evaporation. It exhibits an underpressure during the constant drying period, followed by a steady increase and overpressure during the falling rate drying period. The underpressure in wood occurs when the flow of free water moving towards the surface is greater than the air flow infiltrating from the outside due to lower permeability, in which it may cause the collapse of wood. The temperature begins to increase up to wet bulb temperature 40°C during the constant rate drying period, followed by approaching to the dry bulb temperature 60°C. It is noticed that the effect of growth rings on the temperature gas pressure distributions are not obvious.

5. Concluding Remarks

A numerical simulation for the process of the wood drying has some of difficulties, for instance, tightly coupled equations, highly non-linear equations, non-linear boundary conditions, steep moisture and pressure gradients, highly convective internal gaseous flows and outer and inner iteration stages make another stumbling block.

In this study we find a appropriate method, so called control volume finite element method, which is convenient to non-dimensionalise the system of equations, and makes an unstructured meshing for processing possible. Also it has a number of different alternatives for the exact shape of CV and is flexible for evaluating fluxes through faces.

A complete CVFE method is suitable for resolving nonlinear transport equations on one-dimensional meshes.

References

1. Baliga and S. V. Patankar, *A New Finite Element Formulation for Convection-Diffusion Problems*, Numerical Heat Transfer **3** (1980), 393–409.

2. W. J. Ferguson, *A Control Volume Finite Element Numerical Simulation of the high temperature drying of Spruce*, Drying Technology **13** (1995), 607–634.

3. S. V. Patankar, *Numerical heat transfer and fluid flow*, Hemisphere Publ. Corp., New York, 1980

4. P. Perré, *Le Séchage convectif de bois résineux: choix, validation et utilisation d'un modéle*, PhD thesis, University Paris VII, 1987

5. P. Perré and I. W. Turner, *A 3-D version of TransPore : a comprehensive heat and mass transfer computational model for simulating the drying of porous media*, International Journal of Heat and Mass Transfer **42** (1999), 4501–4521.

6. P. Perré and I. W. Turner, *The use of macroscopic equations to simulate heat and mass transfer in porous media*, Mathematical Modeling and Numerical Texhniques in Drying Technology Edited by I. Turner and A. S. Mujumdar, Marcel Dekker, New York, (1996), 83–156.

7. I. W. Turner, *The modelling of combined microwave and convective drying of a wet porous material*, PhD thesis, University of Queensland, 1991

8. I. W. Turner and W. J. Ferguson, *An unstructured mesh cell-centered control volume method for simulating heat and mass transfer in porous media: Application to softwood drying*, Applied Mathematical Modelling **11** (1995), 654–674.

9. I. W. Turner and P. Perré, *The use of implicit flux limiting schemes in the simulation of the drying process*, Applied Mathematical Modelling **25** (2001), 513–540.

10. I. W. Turner and P. Perré, *A synopsis of the strategies and efficient resolution techniques used for modelling and numerically simulating the drying process*, Mathematical Modeling and Numerical Texhniques in Drying Technology Edited by I. Turner and A. S. Mujumdar, Marcel Dekker, New York, (1996), 1–82.
11. S. L. Truscott and I. W. Turner, *Heterogeneous three-dimensional computational model for wood drying*, Applied Mathematical Modelling **29** (2005), 381–410.
12. S. Whitaker, *Simultaneous heat, mass, and momentum transfer in porous media : A theory of drying*, Advances in Heat Transfer **13** (1977), 119–203.
13. S. Whitaker, *Heat and mass transfer in granular porous media*, In Advances in Drying 1, Mujumdar, A. S. (Ed.), Hemisphere Publ. Corp., Washington DC, 1980, pp.23-61

DIVISION OF MATHEMATICS AND STATISTICAL INFORMATICS (INSTITUTE OF APPLIED STATISTICS), CHONBUK NATIONAL UNIVERSITY, CHONBUK, 561-756, REPUBLIC OF KOREA
  E-mail address: lyh229@chonbuk.ac.kr

DEPARTMENT OF FOREST PRODUCTS, COLLEGE OF AGRICULTURE, CHONNAM NATIONAL UNIVERSITY, GWANGJU, 500-757, REPUBLIC OF KOREA

DEPARTMENT OF FOREST PRODUCTS, COLLEGE OF AGRICULTURE, CHONNAM NATIONAL UNIVERSITY, GWANGJU, 500-757, REPUBLIC OF KOREA